Gaining ligand selectivity in thyroid hormone receptors via entropy

Leandro Martínez[a,1], Alessandro S. Nascimento[b,1], Fabio M. Nunes[b], Kevin Phillips[c], Ricardo Aparicio[b,2], Sandra Martha G. Dias[b,3], Ana Carolina M. Figueira[b], Jean H. Lin[c], Phuong Nguyen[c], James W. Apriletti[c], Francisco A. R. Neves[d], John D. Baxter[c,4], Paul Webb[c,4], Munir S. Skaf[a,4], and Igor Polikarpov[b,4]

[a]Instituto de Química, Universidade Estadual de Campinas, SP 13084-862, Campinas, Brazil; [b]Instituto de Física de São Carlos, Departamento de Física e Informática, Universidade de São Paulo, SP 13566-590, São Carlos, Brazil; [c]Methodist Hospital Research Institute, Houston, TX 77030; and [d]Laboratório de Farmacologia Molecular, Faculdade de Ciências de Saúde, Universidade de Brasília, Campus Universitário Darcy Ribeiro, DF 70910-900, Brasília, Brazil

Contributed by John D. Baxter, October 12, 2009 (sent for review September 8, 2008)

Nuclear receptors are important targets for pharmaceuticals, but similarities between family members cause difficulties in obtaining highly selective compounds. Synthetic ligands that are selective for thyroid hormone (TH) receptor β (TRβ) vs. TRα reduce cholesterol and fat without effects on heart rate; thus, it is important to understand TRβ-selective binding. Binding of 3 selective ligands (GC-1, KB141, and GC-24) is characterized at the atomic level; preferential binding depends on a nonconserved residue (Asn-331β) in the TRβ ligand-binding cavity (LBC), and GC-24 gains extra selectivity from insertion of a bulky side group into an extension of the LBC that only opens up with this ligand. Here we report that the natural TH 3,5,3′-triodothyroacetic acid (Triac) exhibits a previously unrecognized mechanism of TRβ selectivity. TR x-ray structures reveal better fit of ligand with the TRα LBC. The TRβ LBC, however, expands relative to TRα in the presence of Triac (549 Å^3 vs. 461 Å^3), and molecular dynamics simulations reveal that water occupies the extra space. Increased solvation compensates for weaker interactions of ligand with TRβ and permits greater flexibility of the Triac carboxylate group in TRβ than in TRα. We propose that this effect results in lower entropic restraint and decreases free energy of interactions between Triac and TRβ, explaining subtype-selective binding. Similar effects could potentially be exploited in nuclear receptor drug design.

Triac | design | mobility

Nuclear receptors (NRs) are conditional transcription factors with important roles in development and disease (1, 2). Although these proteins are targets for existing drugs and pharmaceutical development, structural relationships between subsets of these proteins mean that ligands that target one NR can cross-react with others. This is commonly observed when NRs exist in multiple subtypes, as for thyroid hormone (TH) receptors (TRs), estrogen receptors (ERs), and peroxisome proliferator receptors, but can be a problem with steroid hormone receptors and other closely related receptors.

TH excess leads to cholesterol lowering and fat loss and undesirable effects (altered heart rate, muscle wasting, and bone resorption) (3). There are 2 TRs (TRα and TRβ) encoded by different genes. They bind the major active TH (3,5,3′triiodo-L-thyronine, T_3) with similar affinities but evoke different responses on activation: TRβ mediates beneficial effects on cholesterol, whereas TRα mediates harmful effects on heart (3, 4). Synthetic TRβ-selective ligands, some of which exhibit liver-selective uptake, reduce serum cholesterol and other atherogenic lipids in preclinical animal models (reviewed in ref. 4). The ligands also reduce body fat without effects on lean muscle in rodents and primates, enhance aspects of reverse cholesterol transport in mice, and improve blood glucose levels in mouse models of type 2 diabetes (4). Two ligands, GC-1 and KB2115, have entered human trials, and the latter has been tested in humans, where it reduces serum LDL cholesterol, lipoprotein(a), and triglycerides (4, 5).

It remains important to develop compounds with larger therapeutic windows between good and bad effects. Binding modes of 3 selective ligands (Fig. 1) have been characterized at the atomic level. The TR ligand-binding cavity (LBC), like that of other NRs, lies in the core of the C-terminal ligand-binding domain (LBD) (6). TRβ-selective binding of GC-1 (≈5-fold) and KB141 (≈10-fold) is dependent on a single TR subtype-specific residue in the LBC, TRβAsn-331 and TRαSer-277 (7, 8). These lie in a hydrophilic region of the LBC that contacts charged groups of the T_3 amino propionate group, and pocket swap mutations that reverse the identity of these residues also reverse TR preference for GC-1 and KB141. X-ray structural analysis indicates that TRβAsn-331 repositions Arg-282 relative to its TRα equivalent (Arg-228), and this facilitates hydrogen bond formation between the Arg-282 side chain and the GC-1 or KB141 carboxylate group (7–9). TRβ-selective binding of GC-24 (≈40-fold) is partly dependent on Asn-331β but involves another mechanism (10); ligand occupies the LBC and conserved hydrophobic regions of helices (H) 3 and 11 open to form an extension to the LBC that accommodates a bulky GC-24 phenyl group. The TRβ H3–H11 region is more flexible than that of TRα in crystal structures, likely explaining subtype selectivity.

Triac is a TR agonist that binds 2–3-fold selectively to TRβ in vitro (11), only moderately less than GC-1. The mechanism of selective Triac binding has not been explored. In fact, though not previously emphasized, initial comparisons of moderate resolution x-ray structures of rat (r) TRα and human (h) TRβ LBDs with Triac suggested that Triac fits the TRα LBC better than TRβ (6).

In this study, we explored this apparent paradox using new high-resolution structures of hTR-Triac complexes and molecular dynamics (MD) simulations. MD simulations have accurately described TR LBD dynamics (12–15), and predicted interaction energies of TR/GC-1 and TR/KB141 complexes support the concept that TRβ makes stronger contacts with GC-1 and KB141 carboxylate groups than TRα, and that Arg-282β position is important for this effect (9). Here, simulations

Author contributions: L.M., A.S.N., F.A.R.N., J.D.B., P.W., M.S.S., and I.P. designed research; L.M., A.S.N., F.M.N., K.P., R.A., S.M.G.D., A.C.M.F., J.H.L., P.N., J.W.A., and P.W. performed research; L.M., A.S.N., F.M.N., R.A., S.M.G.D., J.D.B., P.W., and M.S.S. analyzed data; and L.M., A.S.N., J.D.B., P.W., and M.S.S. wrote the paper.

Conflict of interest: J.D.B. has proprietary interests in Karo Bio AB, which has commercial interests in this area of research.

Data deposition: Coordinates and structure factors have been deposited in the Protein Data Bank, www.pdb.org [PDB ID codes 3JZB (TRα-Triac) and 3JZC (TRβ-Triac)].

[1]L.M. and A.S.N. contributed equally to this work.

[2]Present address: Instituto de Química, Universidade Estadual de Campinas, Cx. P. 6154, Campinas, SP 13084-862, Brazil.

[3]Present address: C3–137, Molecular Medicine, College of Veterinary Medicine, Cornell University, Ithaca, NY 14853.

[4]To whom correspondence may be addressed. E-mail: ipolikarpov@if.sc.usp.br, skaf@iqm.unicamp.br, pwebb@tmhs.org, or jbaxter918@aol.com.

This article contains supporting information online at www.pnas.org/cgi/content/full/0911024106/DCSupplemental.

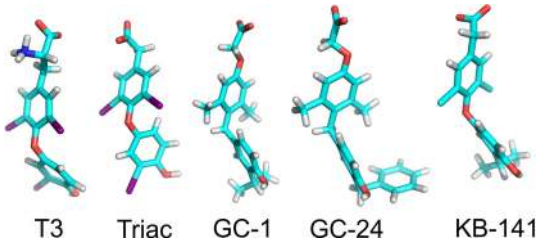

Fig. 1. T_3, Triac, and selective thyromimetics GC-1, GC-24, and KB141.

confirm that the TRα LBC makes stronger direct contacts with Triac than TRβ. However, we also find that the Triac-TRβ complex LBC is larger than the Triac-TRα complex and that this permits greater ligand solvation and increased flexibility of the Triac carboxylate group in TRβ. We propose that entropic contributions of these effects account for selective binding and that similar effects could be exploited in design of NR ligands.

Results

Triac Selectively Binds TRβ. We examined Triac interactions with hTRs (Fig. 2). We used equilibrium ligand binding assays to measure competition with [^{125}I]T_3 for hTR binding. Fig. 2*A* shows that the competition curve is leftward shifted with Triac relative to T_3 with TRβ but not TRα, reflective of higher Triac affinity for TRβ. The ratio of T_3 to Triac IC_{50} values was 0.97 ± 0.09 with TRα and 2.94 ± 0.52 with TRβ (Fig. 2*A*, *Inset*), consistent with previous estimates of TRβ-selective binding (6, 11). As seen for GC-1 and KB141 (7–9), mutations that reverse the subtype-specific TR LBC residue (hTRβ-Asn331Ser and hTRα-Ser277Asn) reverse subtype-specific binding of Triac (Fig. 2*B*). Analysis of thermal denaturation curves of TR-ligand complexes also revealed that Triac stabilizes TRβ more efficiently than TRα (Fig. S1, Table S1) and that Triac protects the TRβ LBD against denaturation more effectively than other ligands, suggesting that the Triac-TRβ complex is particularly stable (see *Discussion*).

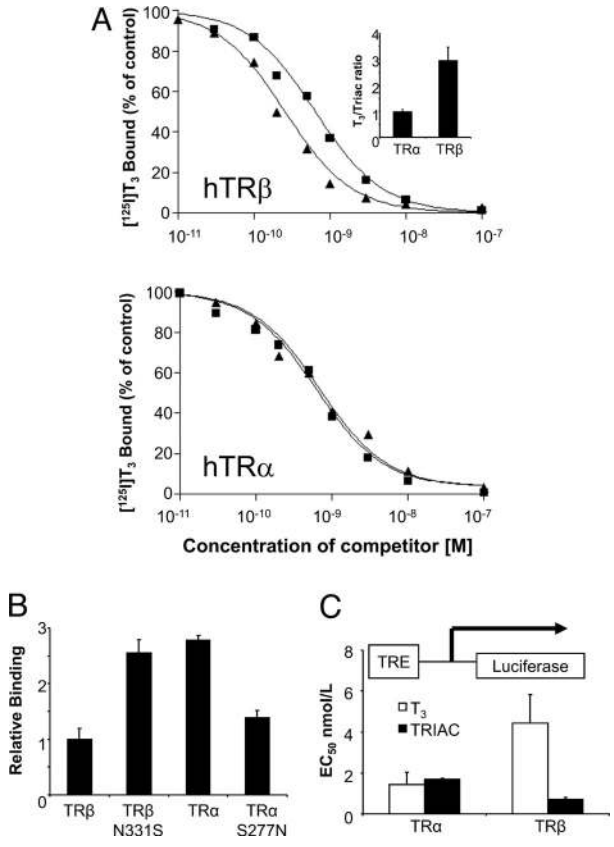

Fig. 2. TR subtype-selective binding and activity of Triac. (*A*) Competition curves with TRβ and TRα obtained with T_3 (squares) and Triac (triangles). *Inset*: Ratios of T_3/Triac binding for both TRs from several experiments (n = 3). (*B*) Relative K_I values from Triac competition curves (n = 4) with TRs and TR mutants were compared with TRβ, arbitrarily set to 1. (*C*) Average EC_{50} values from luciferase assays using extracts of TRα- and TRβ-expressing cells transfected with a TRE-responsive reporter (DR-4) and treated with ligand (n = 3).

Selective activation of TRβ by Triac was detectable in cell culture (Fig. 2*C*). There was a leftward shift in Triac dose–response with TRβ relative to TRα at a thyroid response element (TRE)-driven reporter. Average Triac EC_{50} values were 1.5 nM for TRα and 0.5 nM for TRβ, yielding 3-fold TRβ selectivity. T_3 was 2.3-fold selective for TRα in this system (EC_{50} values were 1.5 and 4.2 nM for TRα and TRβ, respectively). Thus, Triac was approximately 6-fold more potent than T_3 with TRβ.

Triac Makes More Contacts with TRα. We obtained new high-resolution x-ray structures of human TR LBDs with Triac. Previous x-ray structures of TR LBDs with this ligand (7) were of different species (rTRα and hTRβ) and obtained at moderate resolution (2.5 Å). Our hTRα-Triac structure was obtained at higher resolution (2.0 Å; Table S2). We also obtained a new hTRβ structure at similar resolution to the previous one (2.5 Å) but with increased data redundancy to facilitate the assignments of side chain positions (Table S2).

Relationships between Triac and the hTRα LBC are shown in Fig. 3*A* and Table 1. Interactions with Triac thyronine rings with the LBC are mostly hydrophobic, except for contacts between His-381α and the Triac 4′ hydroxyl group. The Triac carboxylate group interacts with the hydrophilic region of the LBC, including one interaction not seen in the rTRα structure: the Ser-277α side chain hydroxyl forms a water-mediated hydrogen bond with an amine group of the Arg-228α side chain which, in turn, forms a water-mediated hydrogen bond with the Triac carboxylate. The structure also confirms previous reports that the Ser-277α main chain amine and both Arg-266α side chain amines form direct hydrogen bonds with the Triac carboxylate.

As in previous hTRβ-Triac structures, Asn-331β hydrogen bonds with Arg-282β, repositioning the Arg-282β side chain away from ligand. This differs from Arg-228α, which forms the water-mediated hydrogen bond with Triac, mentioned above (Fig. 3*A*). The new structure also reveals a unique aspect of TRβ organization: Arg-320β adopts 2 conformations. The first (Arg320A, productive; Fig. 3*B*) resembles the previous hTRβ structure (7); one amine group of the Arg-320 side chain forms a hydrogen bond with the Triac carboxylate group that seems weak because of poor geometry. The second (Arg320B, nonproductive; Fig. 3*B*) was not previously detected; here, the Arg-320 side chain rotates away from ligand. Both conformations differ from hTRα, where Arg-266α side chain amines form well-positioned hydrogen bonds with Triac. B-factors of both conformations of the Arg-320β side chain (48.5 Å^2 and 50.6 Å^2 for A and B conformations) are comparable to each other and neighboring LBC side chains, such as Arg-282 (52.3 Å^2) and Arg-316 (40.9 Å^2), and lower than Triac (74.4 Å^2), suggesting that assignment of double conformation to this residue is realistic.

Together, our x-ray structures suggest that fit of Triac into the TRα LBC is better than the hTRβ LBC (Table 1), contrary to predictions about the nature of TRβ-selective ligand binding (7). The Triac carboxylate forms 4 hydrogen bonds with the hydrophilic portion of the hTRα LBC but only makes 2, at best, with the equivalent region of hTRβ. Of these, the Arg-320β interaction with the Triac carboxylate is weak because of poor alignment in the A conformation and is broken in the B conformation.

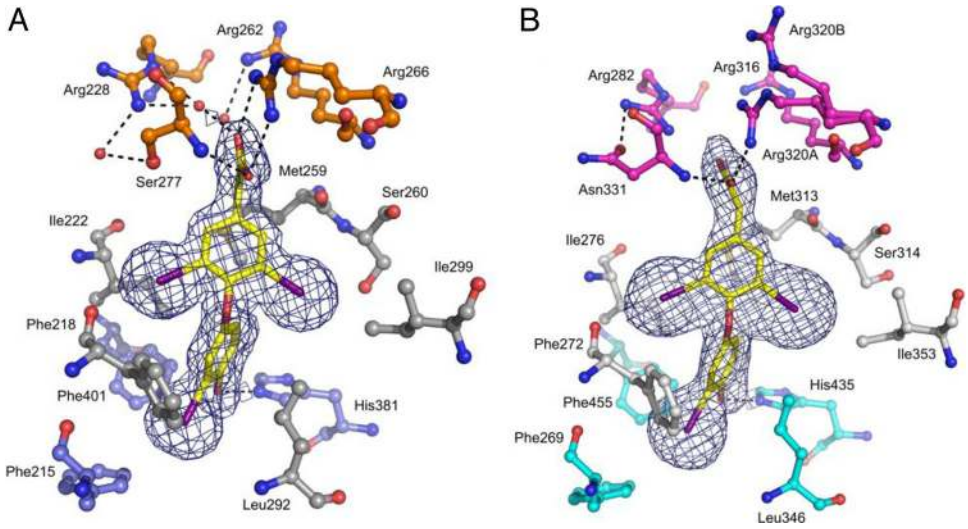

Fig. 3. Better fit of Triac to the TRα LBC. (*A* and *B*) Triac interactions with the TR LBCs. Triac is yellow, with electronic density contoured at 1.0 ó. Hydrogen bonds between the Triac carboxylate group and TRs are shown as dotted lines and waters are shown as red balls. (*A*) Regions of hTRα LBC are in different colors: blue, amphipathic; gray, hydrophobic; and orange, hydrophilic. (*B*) Equivalent region of hTRβ LBC. Cyan, amphipathic; gray, hydrophobic; and purple, hydrophilic. The 2 conformations of Arg-320 are overlaid: A, productive; B, nonproductive.

TR-specific differences in LBC side chain position affect LBC volume around the Triac carboxylate (Fig. 4 *A*–*C*). Calculated LBC volume for TRα is 461 Å^3, whereas volumes for TRβ in the A and B states are 500 Å^3 and 549 Å^3, respectively. Changes in side chain positions in TRβ vs. TRα, illustrated by arrows, account for these alterations. Asn-331β-Arg-282β interactions that retract the Arg-282β side chain increase TRβ LBC volume in the productive state relative to TRα (Fig. 4 *A* and *B*). Repositioning of Arg-320β in the B conformation accounts for the further increase in TRβ LBC volume (Fig. 4 *B* and *C*). Similar effects are not seen with TR-T_3 structures (Fig. S2); here, Arg-282β and Arg-228α side chains interact directly with ligand, resulting in identical LBC configuration and volume.

Water Compensates for Weaker TRβ-Triac Interactions. To determine why Triac is TRβ selective, we conducted MD simulations to estimate interaction energies of ligand with TRs and observe dynamics. The simulations used new hTRα and hTRβ-Triac structures and included a shell of water and ions to reproduce solution conditions. Computation of interaction energies of both TRs and Triac confirms the impressions obtained from x-ray structures: TRα makes stronger direct contacts with ligand (Fig. S3, Table 2). Interaction energies of Triac with TRα were approximately 20 kcal mol^{-1} stronger than with TRβ. However, calculation of Triac interaction energies with the complete system (protein + water + ions) revealed no difference (Fig. S3, Table 2); interaction energies of Triac with water in the TRβ LBC are stronger than with TRα (Table 2) and compensate for weaker direct interactions of TRβ with Triac.

Fig. 5*A* shows all 5 water molecules that engage in strong favorable interactions (pair energy ≈ -10 kcal mol^{-1}) with Triac during the TRα simulation; each colored trace corresponds to a different water molecule. At the beginning, only 1 molecule (red) interacts strongly with Triac (favorable interactions). This molecule (red) is replaced by another (blue, first arrow), returns (second arrow), and subsequently is replaced by others (green, third arrow; tan, fourth arrow; black). Thus, only 1 water molecule interacts with Triac at each instant of the simulation, and there is constant exchange of the individual molecules in this position. Analysis of individual simulation timeframes reveals that the water molecule that interacts strongly with Triac cor-

Table 1. Interaction distances of hydrogen bonds between Triac and TR LBCs

HTRα	Distance (Å)	hTRβ	Distance (Å)
His381	2.62	His435	2.77
Arg266-NH1	3.16	Arg320A-NH1	3.06
Arg266-NH2	3.16	—	—
Ser277	2.83	Asn331	2.63
HOH	2.43	—	—

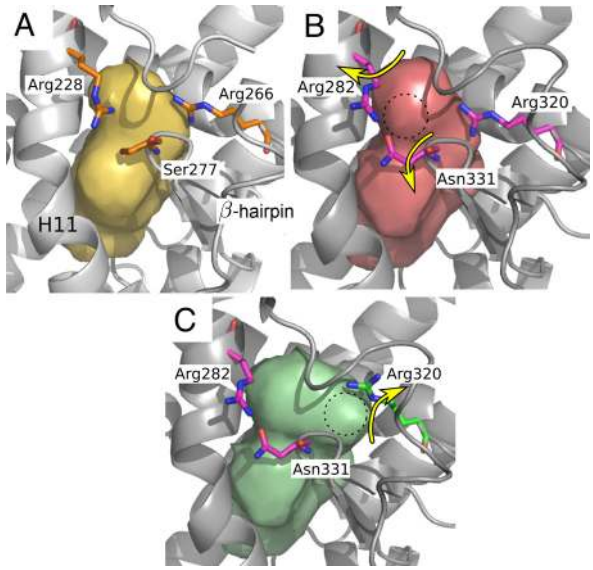

Fig. 4. TRβ LBC is larger than the TRα LBC with Triac. (*A*) Ribbon diagram of TRα showing the LBC in gold space-filling form. Side chains of key Arg residues are shown. (*B*) Similar view of TRβ LBC (pink) with Arg-320 in the productive (A) conformation and movements of TRβN331 and TRβR282 side chains that lead to altered LBC volume relative to TRα (yellow arrows). Note increased volume at the top of the LBC relative to TRα in *A* (dotted circle). (*C*) TRβ LBC (green), with Arg-320 in nonproductive B conformation and movement of the Arg-320 side chain relative to productive A conformation. Note increased volume on the top right of the LBC relative to TRβ in *B* (dotted circle).

Table 2. Interaction energies of Triac within MD simulations

Interaction with:	TRα /kcal mol^{-1}	TRβ /kcal mol^{-1}
LBD residues	−66.63	−46.96
Whole environment	−192.74	−192.52
Waters	−18.37	−37.56

responds to the molecule that forms the water-mediated hydrogen bond contact between Arg-228α and Triac, seen in our high-resolution hTRα x-ray structure (Fig. 5*C*).

By contrast, Triac interacts strongly with several waters in the TRβ LBC (Fig. 5*B*). At the beginning, 2 waters (green, blue) interact with Triac. As the simulation evolves, another (red) joins the first 2, and at subsequent times either 3 or 4 water molecules are found in the LBC (favorable interactions). As seen with TRα, individual waters fluctuate between low- and high-energy states (events marked by arrows), implying continuous exchange between positions near Triac in the LBC and the external hydration shell. Visualization of relevant interacting water molecules confirms that they lie close to the Triac carboxylate. A representative frame from the simulation (Fig. 5*D*) reveals 3 water molecules in contact with Triac, with 2 nearby, all of these molecules displaying high mobility throughout the simulation. We conclude that several waters occupy the space in the TRβ LBC near the Triac carboxylate group and bridge charged groups of ligand and TRβ protein, explaining how water compensates for weaker direct interactions between TRβ and Triac (Table 2; see *Discussion*).

We also performed simulations with TRα and TRβ structures in which side chains of subtype-specific LBC residues S277 and N331 were exchanged to create computational builds of TR LBC mutants. These simulations lend further support to the notion that TRβN331 regulates LBC volume and water content in the presence of Triac (Fig. S4). TRα-S277N and TRβ-N331S mutant

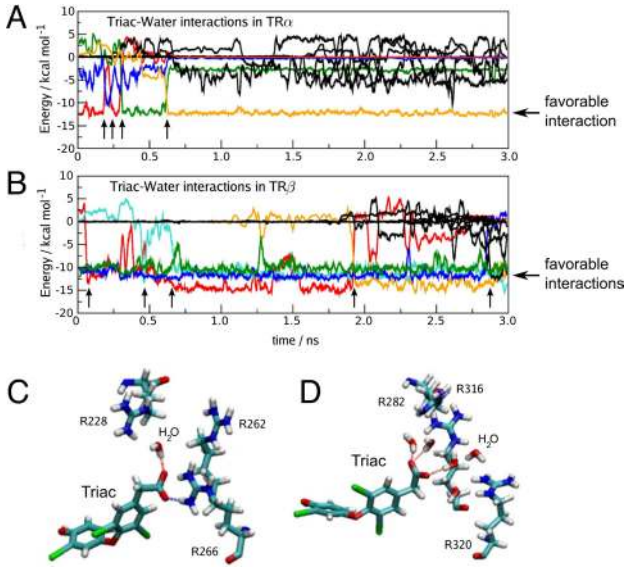

Fig. 5. Triac makes more water contacts in TRβ. Interaction energy profiles of most favorable interacting water molecules obtained from MD simulation (*A*) hTRα and (*B*) hTRβ. Each colored trace represents interaction energies of different water molecules with Triac as a function of time. Arrows indicate water exchange events. Representative views of key amino acids in the hTRα (*C*) and hTRβ (*D*) LBCs and nearby space in the LBC from the simulation, showing higher hydration level in TRβ and that highly favorable interacting waters lie close to the Triac carboxylate. Waters are represented by white/red stick figures, and hydrogen bond interactions with Triac are represented by dotted lines. Note that there are more waters close to the Triac molecule in TRβ than in TRα.

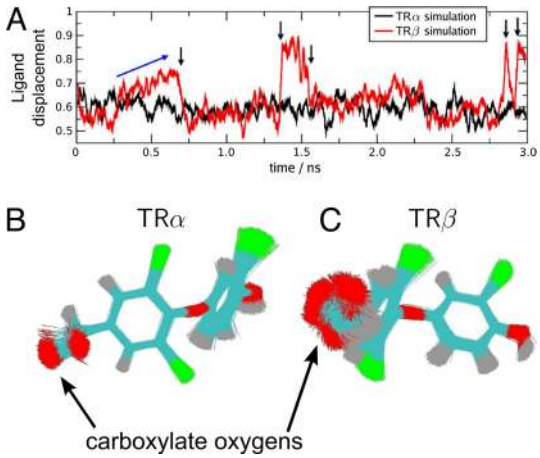

Fig. 6. Triac is more mobile in the TRβ LBC. (*A*) Ligand displacement of Triac over time. RMSD per atom for Triac bound to hTRα (black) and hTRβ (red) as a function of time over the simulation. Arrows show Triac conformational transitions in TRβ: blue arrow, a smooth transition; black arrows, sharp transitions. (*B*) hTRα LBC and (*C*) hTRβ LBC indicating increased mobility of the carboxylate in TRβ over time. The figures are composed of superimposed Triac conformations from all frames of the simulations. Red, oxygen; green, iodine. The wide distribution of atoms corresponding to the Triac carboxylate oxygens are indicated by the larger space (red).

LBCs acquire some characteristics of the other subtype: there is reversal of Arg-228α/Arg-282β position, subtype-specific changes in pocket volume, and water is expelled from the TRβ-N331S LBC (Fig. S4 *a–c*).

Triac Flexibility in TRs. Water compensation of the interaction energies cannot, alone, explain Triac TRβ selectivity. However, Triac exhibits increased mobility in the TRβ vs. TRα LBC, as indicated by the overall rmsd of Triac atoms. Triac is relatively restricted in TRα, and the ligand oscillates with rmsd amplitudes between 0.5 and 0.7 Å (Fig. 6*A*). By contrast, Triac exhibits 1 long smooth transition and 5 sharp variations in rmsd in TRβ (Fig. 6*A*, blue and black arrows).

Analysis of individual Triac atoms indicates that the carboxylate oxygens are more mobile (0.011 Å ps^{-1}) in TRβ vs. TRα. (Fig. S5*A*), owing to increased carboxylate group rotation. Superimposed frames of the simulation reveal that carboxylate oxygens (red) oscillate around well-defined positions in TRα but are delocalized in TRβ (Fig. 6 *B* and *C*). T_3 did not exhibit similar movements with either TR (Fig. S5*B*). We estimated the conformational entropy gain of Triac in TRβ vs. TRα from the simulations using an adapted colony potential energy calculation method (ref. 16; *SI Text*, Figs. S6–S8). Predicted conformational entropy gain of Triac in TRβ is 1.5 cal K^{-1} mol^{-1}, implying a free energy difference of −0.44 kcal mol^{-1}, which accounts for the 2–3-fold TRβ selectivity of Triac (implied free energy difference −0.45 to −0.65 kcal mol^{-1}).

Discussion

In this study, we used biochemical and x-ray structural analysis and MD simulations to investigate Triac interactions with TRs. Triac is a natural TH that displays selective actions in humans (17); it exhibits cholesterol-lowering activities (typically TRβ dependent) that are separable from other TR-regulated parameters including heart rate (TRα dependent). Thus, better understanding of Triac selectivity is relevant for understanding of TR activation and thyromimetic action in vivo.

We confirm that Triac is approximately 3-fold TRβ selective in vitro (7, 11), close to estimates for GC-1 (4). In addition, we show moderate TRβ selectivity in cell culture and find that

selective binding of Triac to TRβ is dependent on the nonconserved TRβ-LBC residue (Asn-331), like GC-1 and KB141 (7–9). However, x-ray structural data indicate that Triac is not simply a less-selective version of existing compounds; analysis of x-ray structures of hTR-Triac complexes reveals better fit of ligand to the TRα LBC, and this is confirmed by TR protein-Triac interaction energies in our MD simulations, opposite to the case for GC-1 and KB141 (7–9).

Closer analysis of TR x-ray structures coupled with analysis of water and ligand dynamics in MD simulations provides a likely explanation for this apparent paradox. Differences in TRβ and TRα LBC amino acid side chain positions that occur with Triac and not T_3 lead to a TRβ/Triac complex-specific expansion of pocket volume. The LBC in the TRα-Triac complex is smaller than TRβ and contains space for 1 water molecule near the Triac carboxylate. By contrast, the same region of the TRβ LBC accommodates 2 to 5 waters. Our calculations indicate that improved water contacts compensate for weaker direct TRβ interactions with ligand; water molecules act as bridges between ligand and protein (Table 2). The waters also allow the Triac carboxylate group more flexibility in the TRβ LBC than TRα; Triac carboxylate oxygens are approximately twice as flexible in TRβ (Figs. 5*B* and S5*A*). Because interaction energies of Triac with both TR systems (protein + water + ions) are similar, we surmise that increases in free energy of association of Triac with TRβ stem from the entropic contribution of increased ligand flexibility. Indeed, calculations of entropic gain of Triac binding to TRβ based on observed ligand flexibility in simulations (16) agree with binding preferences of Triac for TRβ.

To our knowledge, entropic effects have not been explicitly invoked to explain subtype-selective binding of synthetic TR or NR ligands. It is clear that such effects play important roles in several protein–ligand interactions (18, 19); examples include improved inhibitor binding (20, 21) and many other aspects of protein/small molecule interactions, such as ligand dissociation paths (22) and ion permeation (23). It is interesting to evaluate previous NR structures in the light of our results. TRβ selectivity of GC-24 stems mostly from the extension of the LBC, but Asn-331β also contributes to selectivity, and contacts between the GC-24 carboxylate and this part of the LBC seem to be suboptimal (10). Thus, entropic influences could contribute to selective binding of GC-24. Improved affinity of vitamin D receptor ligands has been associated with factors shown to be important here, including water in the LBC (24), increased LBC volume, and multiple ligand conformations (25–27). Two groups, including ours, found that water can substitute for charged regions of NR LBCs at little or no energetic cost in MD simulations, lending support to the idea that water substitutes for loss of direct protein contacts (17, 18, 28). However, perhaps the best example of links between entropic contributions and subtype selectivity may come from binding modes of the ER ligand THC [(R,R)-5,11-*cis*-diethyl-5,6,11,12-tetrahydrochrysene-2,9-diol], a selective agonist that binds ERβ with 4-fold higher affinity and antagonizes ERα (29). X-ray structures reveal that the ERβ LBC, generally smaller than ERα, expands with THC to reduce direct ligand contacts (30). This seems strongly analogous to the TR-Triac case.

It will be important to assess entropic and enthalpic contributions to TR ligand binding affinity in vitro. Classically, this is addressed with isothermal titration calorimetry, which measures heat variation (ΔH) from a system at set temperature and free energy of ligand association (ΔG). Standard versions of this approach rely on rapid ligand binding (<1 s), but NR ligand association kinetics are slow (31). It is theoretically possible to correct for this effect by extending the experiment, but lability of standard TR preparations over long times at higher temperatures and the hydrophobic nature of ligands precludes reliable results. We continue to work on this problem, but one piece of experimental evidence favors an entropic contribution to Triac binding: the TRβ-Triac complex is more resistant to thermal denaturation than the equivalent TRβ-T_3 complex (Fig. S1). Such effects have previously been linked to entropic contributions in free energies of ligand association (23, 32).

Our observations imply that standard approaches to improve TR and NR ligand binding by increasing complementarity of ligand and LBC may not identify the tightest binding or most selective ligands. Will it be possible to use enthalpy/entropy compensation for design of new TRβ-selective thyromimetics? Rational consideration of enthalpy and entropy in ligand binding is a difficult issue (33). However, combinations of biochemical/structural analysis and MD simulations could permit intelligent approaches. Ye et al. (8) found that TRβ selectivity of Triac was reduced from 2.9 to 1.3 with a larger 1-substituent in L-3′5′3′-triiodothyropropionic acid. Given that the Triac carboxylate group improves ligand selectivity because it explores more conformations at this position in the larger pocket, it may be possible to exploit entropic influences in NR ligand design by targeted reduction of substituent size near regions of the LBC that can vary in volume.

Materials and Methods

Protein Purification. hTRβ LBD (202–461) and hTRα LBD (148–410) were expressed as described previously (34). Ligand was added to 5-fold excess after cell disruption by sonication. Both proteins were concentrated by centrifugation before crystallization.

Ligand Binding. T_3 and Triac binding affinities were determined by saturation binding assays as described previously (35). HeLa cells that express TRα or TRβ were transfected with a DR-4 element-driven luciferase reporter (35).

Protein Crystallization and Data Collection. hTRα1 crystals grew in conditions previously described (34). hTRβ1 crystals grew in conditions established for other hTRβ complexes (7). Datasets were collected using a Mar345dtb image plate mounted at a Rigaku rotating anode X18 source equipped with Osmic Confocal MaxFlux mirrors operating with CuKα radiation. During data collection, crystals were kept on a nitrogen stream at 100 K.

Structure Solution. Datasets were reduced and merged using MOSFLM/SCALA. Structures of hTRα LBD and hTRβ LBD with Triac were solved by molecular replacement using TR-T_3 complexes as search models. Molecular replacement used MOLREP, and structures were refined using REFMAC and PHENIX. To gain in precision of measurements of reflection intensities and to obtain a robust data for x-ray structure refinement, we measured redundant datasets for hTRα and hTRβ crystals (Table S2).

MD Simulations. New hTRα and hTRβ structures with Triac were used. Simulated systems contained LBD, Triac, and a 15-Å-thick solvation layer with 16,500 water molecules and counter ions. Water and ions were added with Packmol (36), and 3-ns-long simulations were performed with NAMD (37) using CHARMM parameters (38). Ligand parameters and the protocols for equilibration and simulations are described in ref. 14. Binding cavities and volumes were computed using VOIDOO (39). Figures of molecular structures were prepared with Pymol (40).

ACKNOWLEDGMENTS. We thank R. Portugal, M. Nakamura, A. Bernardes, and F. Batista for help in data measurement. Supported by Conselho Nacional de Desenvolvimento Científico e Tecnológico (Grant 06/00182–8); Fundação de Amparo à Pesquisa do Estado de São Paulo; National Institutes of Health (Grants DK41482 and DK51281, Ph.D. stipends to A.S.N. and A.C.M.F.); and Coordenação de Aperfeiçoamento de Pessoal de Nível Superior (Ph.D. stipend to F.M.N.).

1. Baxter JD, et al. (2001) Selective modulation of thyroid hormone receptor action. *J Steroid Biochem Mol Biol* 76:31–42.
2. Laudet V, Gronemeyer H (2002) *The Nuclear Receptor Facts Book* (Academic, London).
3. Yen PM (2001) Physiological and molecular basis of thyroid hormone action. *Physiol Rev* 81:1097–1142.
4. Baxter JD, Webb P (2009) Thyroid hormone mimetics: Potential applications in atherosclerosis, obesity and type 2 diabetes. *Nat Rev Drug Discov* 8:308–320.

5. Berkenstam A, et al. (2008) The thyroid hormone mimetic compound KB2115 lowers plasma LDL cholesterol and stimulates bile acid synthesis without cardiac effects in humans. *Proc Natl Acad Sci USA* 105:663–667.
6. Wagner RL, et al. (1995) A structural role for hormone in the thyroid hormone receptor. *Nature* 378:690–697.
7. Wagner RL, et al. (2001) Hormone selectivity in thyroid hormone receptors. *Mol Endocrinol* 15:398–410.
8. Ye L, et al. (2003) Thyroid receptor ligands. 1. Agonist ligands selective for the thyroid receptor β1. *J Med Chem* 46:1580–1588.
9. Bleicher L, et al. (2008) Structural basis of GC-1 selectivity for thyroid hormone receptor isoforms. *BMC Struct Biol* 8:8.
10. Borngraeber S, et al. (2003) Ligand selectivity by seeking hydrophobicity in thyroid hormone receptor. *Proc Natl Acad Sci USA* 100:15358–15363.
11. Schueler PA, Schwartz HL, Strait KA, Mariash CN, Oppenheimer JH (1990) Binding of 3,5,3′-triiodothyronine (T3) and its analogs to the in vitro translational products of c-erbA protooncogenes: Differences in the affinity of the α- and β-forms for the acetic acid analog and failure of the human testis and kidney α-2 products to bind T3. *Mol Endocrinol* 4:227–234.
12. Karplus M, McCammon JA (2002) Molecular dynamics simulations of biomolecules. *Nat Struct Biol* 9:646–652.
13. Martinez L, et al. (2005) Molecular dynamics simulations reveal multiple pathways of ligand dissociation from thyroid hormone receptors. *Biophys J* 89:2011–2023.
14. Martinez L, Webb P, Polikarpov I, Skaf MS (2006) Molecular dynamics simulations of ligand dissociation from thyroid hormone receptors: Evidence of the likeliest escape pathway and its implications for the design of novel ligands. *J Med Chem* 49:23–26.
15. Martinez L, Polikarpov I, Skaf MS (2008) Only subtle protein conformational adaptations are required for ligand binding to thyroid hormone receptors: Simulations using a novel multipoint steered molecular dynamics approach. *J Phys Chem B* 112:10741–10751.
16. Xiang Z, Soto CS, Honig B (2002) Evaluating conformational free energies: The colony energy and its application to the problem of loop prediction. *Proc Natl Acad Sci USA* 99:7432–7437.
17. Sherman SI, et al. (1997) Augmented hepatic and skeletal thyromimetic effects of tiratricol in comparison with levothyroxine. *J Clin Endocr Metab* 82:2153–2158.
18. Ladbury JE (1996) Just add water! The effect of water on the specificity of protein-ligand binding sites and its potential application to drug design. *Chem Biol* 3:973–980.
19. Holdgate GA, et al. (1997) The entropic penalty of ordered water accounts for weaker binding of the antibiotic novobiocin to a resistant mutant of DNA gyrase: A thermodynamic and crystallography study. *Biochemistry* 36:9663–9673.
20. Velazquez-Campoy A, et al. (2000) Thermodynamic dissection of the binding energetics of KNI-272, a potent HIV-1 protease inhibitor. *Protein Sci* 9:1801–1809.
21. Kavanagh KL, et al. (2006) The molecular mechanism of nitrogen-containing bisphosphonates as antiosteoporosis drugs. *Proc Natl Acad Sci USA* 103:7829–7834.
22. Sheu SY (2006) Selectivity principle of the ligand escape process from a two-gate tunnel in myoglobin: Molecular dynamics simulation. *J Chem Phys* 124:154711.
23. Bastug T, Gray-Weale A, Patra SM, Kuyucak S (2006) Role of protein flexibility in ion permeation: A case study in gramicidin. *Biophys J* 90:2285–2296.
24. Hourai S, et al. (2006) Probing a water channel near the A-ring of receptor-bound 1α,25-dihydroxyvitamin D3 with selected 2α-substituted analogues. *J Med Chem* 49:5199–5205.
25. Vaisanen S, Perakyla M, Karkkainen JI, Uskokovic MR, Carlberg C (2003) Structural evaluation of the agonistic action of a vitamin D analog with two side chains binding to the nuclear vitamin D receptor. *Mol Pharmacol* 63:1230–1237.
26. Molnar F, Perakyla M, Carlberg C (2006) Vitamin D receptor agonists specifically modulate the volume of the ligand-binding pocket. *J Biol Chem* 281:10516–10526.
27. Carlberg C, Molnar F (2006) Detailed molecular understanding of agonistic and antagonistic vitamin D receptor ligands. *Curr Top Med Chem* 6:1243–1253.
28. Kosztin D, Izrailev S, Schulten K (1999) Unbinding of retinoic acid from its receptor studied by steered molecular dynamics. *Biophys J* 76:188–197.
29. Sun J, et al. (1999) Novel ligands that function as selective estrogens or antiestrogens for estrogen receptor-α or estrogen receptor-β. *Endocrinology* 140:800–804.
30. Shiau AK, et al. (2002) Structural characterization of a subtype-selective ligand reveals a novel mode of estrogen receptor antagonism. *Nat Struct Biol* 9:359–364.
31. Sandler B, et al. (2004) Thyroxine-thyroid hormone receptor interactions. *J Biol Chem* 279:55801–55808.
32. Waldron TT, Murphy KP (2003) Stabilization of proteins by ligand binding: Application to drug screening and determination of unfolding energetics. *Biochemistry* 42:5058–5064.
33. Freire E (2008) Do enthalpy and entropy distinguish first in class from best in class? *Drug Disc Today* 13:869–874.
34. Nascimento AS, et al. (2006) Structural rearrangements in the thyroid hormone receptor hinge domain and their putative role in the receptor function. *J Mol Biol* 360:586–598.
35. Togashi M, Nguyen P, Fletterick R, Baxter JD, Webb P (2005) Rearrangements in thyroid hormone receptor charge clusters that stabilize bound 3,5′,5-triiodo-L-thyronine and inhibit homodimer formation. *J Biol Chem* 280:25665–25673.
36. Martinez L, Andrade R, Birgin EG, Martinez JM (2009) PACKMOL: A package for building initial configurations for molecular dynamics simulations. *J Comput Chem* 30:2157–2164.
37. Phillips JC, et al. (2005) Scalable molecular dynamics with NAMD. *J Comput Chem* 26:1781–1802.
38. MacKerell AD, et al. (1998) All-atom empirical potential for molecular modeling and dynamics studies of proteins. *J Phys Chem B* 102:3586–3616.
39. Kleywegt GJ, Jones TA (1994) Detection, delineation, measurement and display of cavities in macromolecular structures. *Acta Crystallogr D* 50:178–185.
40. Delano WL (2002) *The PYMOL Molecular Graphics System* (Delano Scientific, Palto Alto, CA).